Fully-Conjugated Donor-Acceptor Block-Copolymers for Organic Photovoltaics via Heck-Mizoroki Coupling

Aiman Rahmanudin,† Liang Yao, Arvindh Sekar, Han-Hee Cho, Yongpeng Liu, Charles R. Lhermitte and Kevin Sivula*

Laboratory for Molecular Engineering of Optoelectronic Nanomaterials, École polytechnique fédérale de Lausanne (EPFL), Station 6, CH-1015, Switzerland

ABSTRACT: The development of facile routes to prepare fully-conjugated block copolymers (BCPs) from diverse monomers is an important goal for advancing robust bulk-heterojunction (BHJ) organic photovoltaics (OPVs). Herein we introduce a synthetic strategy for step-growth BCPs employing 1,2-bis(trialkylstannyl)ethene as one monomer, which, in addition to offering improved backbone planarity, directly yields a vinylene-terminated macromonomer suitable for Heck-Mizoroki coupling. The benefits of our strategy, which facilitates the preparation of functionalized macromonomers suitable for BCP synthesis, is demonstrated with a representative BCP based on a diketopyrrolopyrrole (DPP) copolymer coded pBDTTDPP as the donor block and a perylenediimide (PDI) copolymer coded as pPDIV as the acceptor block. Feed ratio optimization affords control over the macromonomer chain-end functionalities and allows for the selective formation of a tri-BCP consisting of pPDIV-*b*-pBDTTDPP-*b*-pPDIV, which is employed in a single-component BHJ OPV. Devices achieved a power conversion efficiency of 1.51% after thermal stress at 150°C compared to 0.02% for control device consisting of a comparable blend of pBDTTDPP and pPDIV. The difference in performance is ascribed to the morphological stability of the BHJ when using the BCP.

Semiconducting polymer based organic photovoltaics (OPVs), which consist of solution-processed bulk-heterojunctions (BHJs) of electron donating and electron-accepting materials, have reached power conversion efficiency (PCE) suitable for many commercial applications.[1-4] However, the durability of the BHJ remains a factor limiting their widespread implementation.[5-7] In response to this drawback, semiconducting (conjugated) block copolymers (BCPs), which employ covalently linked donor and acceptor blocks, have garnered significant interest to improve the BHJ stability.[8] The attractiveness of BCPs derives from their unique ability to form thermodynamically stable BHJs with tunable domain sizes suitable for optimizing exciton dissociation while also maintaining continuous conduction pathways for charge extraction.[9-13] This offers the possibility of creating highly stable single component (SC)-BHJ OPVs not affected by uncontrollable donor-acceptor phase segregation. Currently, the state-of-art SC-BHJ OPVs employ BCPs with poly-3-hexylthiophene (P3HT) as the donor block.[14-18] Most notably, Gomez and coworkers reported a P3HT-*b*-poly(fluorene-bisthiophene) device that achieved a PCE of 3%.[19] The dependency on using P3HT as a donor block has arisen due to the ease of obtaining well-defined low dispersity, *Đ*, end-functionalized P3HT *via* catalyst transfer polymerization[20-21] that serves as an ideal macromonomer or macroinitiator for the subsequent growth of an acceptor block via Suzuki[22], Stille[23], direct arylation[24] polycondensation, or chain-growth polymerization.[25] However, the band-gap and energy level positons of P3HT both limit its solar light harvesting and restrict the choice of suitable acceptor blocks, thus restricting the performance of SC-BHJ OPVs. Indeed, the (non BCP) state-of-the-art polymer BHJ OPVs employ "push-pull" copolymers with optimized band gaps and energy levels.[26-28] The preparation of these polymers relies on step-growth carbon-carbon cross coupling reactions, typically between "A—A and B—B" type monomers, which inevitably leads to high *Đ* and significantly complicates the preparation of pure well-defined BCPs.[29-32] Despite this, recently a few reports of step-growth (Stille-coupling) protocols used to prepare non-P3HT based BCPs for SC-BHJ OPVs have appeared.[33-34] A summary of synthetic methodology and device performance of reported SC-BHJ OPVs is presented in the Supporting Information (SI, Table S1), and Scheme 1a illustrates a typical strategy towards well-defined and fully conjugated BCPs *via* step-growth polymerization. Controlling the initial monomer feed ratio can afford effective macromonomer end-group control, but the purification and isolation of low *Đ* macromonomers with stable end functionalization is a major challenge. While our group has previously demonstrated that preparatory size exclusion chromatography (prep-SEC) facilitates the purification of Br/Br end-functionalized macromonomers polymerized *via* Stille coupling, unfortunately the purification of a corresponding bis-stannylated macromonomer proved difficult due to the poor stability of this functional group.[35-36] Thus improvement of this approach is required to enable its active use in the development of SC-BHJ OPVs.

One improvement strategy would be to endow these step-growth polymerization reactions with more chain-growth-like character[37] to facilitate the direct preparation of low *Đ* macromonomers. While promising, this approach is not yet universally applicable to all monomer systems. Alternatively, herein we report a novel synthetic strategy to obtain fully conjugated BCPs by utilizing a palladium-catalyzed Heck-Mizoroki coupling reaction between a Br/Br end-functionalized macromonomer and a macromonomer functionalized

with a vinylene end group (See Scheme 1b). Employing a 1,2-bis(trialkylstannyl)ethene monomer unit[38] enables the isolation and purification of a stable low $Đ$ macromonomer directly suitable for Heck coupling, and crucially avoids the need to handle stannylated macromonomers. Moreover, the resulting vinylene subunit provides the recently-shown advantage of inducing planarity along conjugated polymer backbones,[39-41] which is known to aid in the self-assembly and electronic properties of the resulting polymers prepared with this monomer with bulky monomers like rylene diimides. Our prototype BCP prepared with this method is further shown to have photovoltaic activity in a SC-BHJ OPV device with a substantial improvement of BHJ stability over a control device made with a comparable polymer blend.

Scheme 1. Synthetic methodologies for the preparation of fully conjugated BCPs via step-growth polycondensation. (a) previous work, and (b) the method presented in this work.

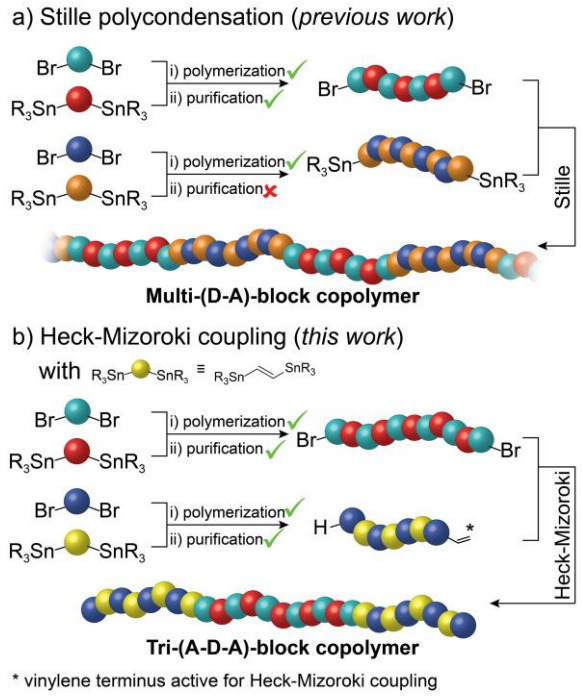

To demonstrate our approach, low-band-gap conjugated polymers coded pBDTTDPP[42] (donor) and pPDIV[39] (acceptor) were selected (see structures in Figure 1a and 1b, respectively) due to their complementary energy levels and absorption spectra suitable for a BHJ OPV device. Moreover, both polymers are known to form highly ordered domains due to their relatively planar conjugated backbone,[43-44] which is essential for driving the BCP self-assembly.[17] To achieve control over the chain-end functionalities, standard Stille polycondensations with a controlled monomer stoichiometry were used to prepare macromonomers with the appropriate terminal groups, i.e. Br/Br end groups for pBDTTDPP and H/vinylene (H/V) for pPDIV as illustrated in Figures 1a and 1b, respectively (See supporting information, SI, for full synthetic details and procedures). Briefly, the donor block pBDTTDPP-(Br/Br) was prepared using a slight excess of the brominated diketopyrrolopyrrole monomer (molar ratio 9:8 with respect to the benzodithiophene monomer). This afforded a crude polymer with a molecular weight M_n = 3.94 kg mol^{-1}, and $Đ$=1.51 as estimated from SEC (See Figure 1c broken blue line). Further purification using prep-SEC gave M_n = 4.20 kg mol^{-1} (a degree of polymerization, DP~3) and $Đ$ = 1.23. Matrix-assisted laser desorption/ionization time-of-flight mass spectrometry (MALDI-TOF MS) analysis confirmed the (Br/Br) end groups (See Figure 1e, and for a zoomed version and tabulated peaks see SI Figure S1 and Table S2), and ^{1}H NMR supports this composition (See SI Figure S2).

Similarly, the acceptor block pPDIV-(H/V) was synthesized with a dibrominated perylenediimide (PDI) and excess 1,2-bis(trimethylstannyl)ethene (molar ratio 8:9). Regioisomerically pure (97%) dibromo-PDI (See SI Figure S3 for characterization) was used to avoid structural defects, which are known to affect π- π stacking and charge transport,[45] and could possibly disrupt the Heck coupling. The SEC trace of the acceptor block synthesis (Figure 1d solid red line) gave M_n = 3.78 kg mol^{-1} (DP~6) and $Đ$=1.21. MALDI-TOF MS confirmed the vinylene end capping on one side of the polymer chain (See Figure 1f and for a zoomed version and tabulated peaks see SI Figure S4 and Table S3).The MALDI-TOF MS analysis also indicated the absence of the end group composition of Br/V, which suggests that dehalogenation occurred similar to previous reports with comparable Stille coupling polycondensation reactions on halogenated rylene-based monomers.[39,46] Moreover, the methyl tin end groups also were not detected as expected due to their instability to purification conditions employed.[35] Fortunately, this lability reveals the vinylene end group suitable for the Heck coupling. We also note the relatively low DPs of both the donor block pBDTTDPP-(Br/Br) and the acceptor block pPDIV-(H/V) would reasonably classify them as oligomers, however, keeping a good solubility of these macromonomers is important for the BCP formation.

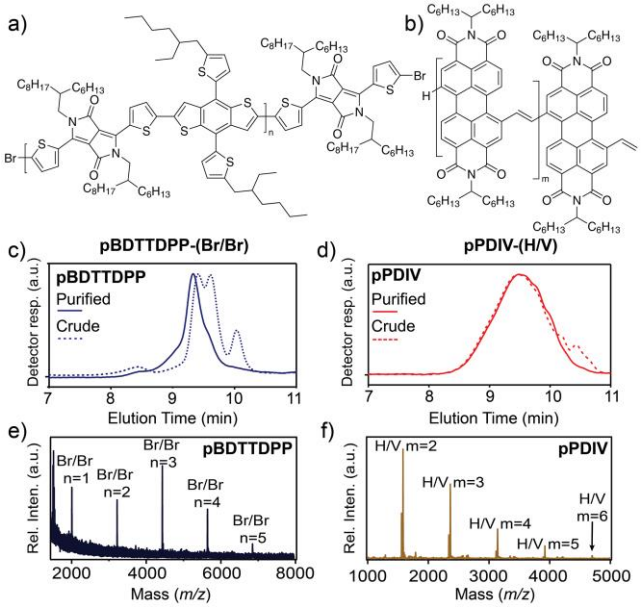

Figure 1. Chemical structures of the donor (a) and the acceptor (b) macromonomers used in this work. Analytical SEC traces (crude and purified) are shown in (c) and (d) for the donor and acceptor, respectively. MALDI-TOF mass spectra analysis of the purified (e) donor and (f) acceptor macromonomers.

To prepare the prototype BCP, a slight excess (molar ratio of 2.3:1) of pPDIV-(H/V) was used to ensure complete reaction at both terminal bromine ends of pBDTTDPP-(Br/Br). The SEC trace of the crude Heck coupling reaction (Figure 2a, broken trace)

indicates a significant increase in M_n as compared to the macromonomers, signaling a successful coupling. After purification by prep-SEC, an estimated M_n = 16.9 kg mol^{-1} ($Đ$ = 1.51) was found which is slightly larger than the value expected for the tri-block copolymer (tri-BCP) from the combined M_n of the macromonomers (11.2 kg mol^{-1}), which is attributed to the purification process. Indeed, after prep-SEC, analytical SEC suggests there is only minimal overlap (~15%) of the molecular weight distribution of tri-BCP with the macromonomers, suggesting that a minor amount of unreacted macromonomers could be present in the purified tri-BCP. Further characterization *via* ^{1}H NMR revealed the presence of proton environments attributed to the aromatic region of the donor block, pBDTTDPP-*b*, and acceptor block, pPDIV-*b* (See Figure 2b for the ^{1}H NMR spectrum region of interest and Figure 2c for the assignment of the protons on the chemical structure of tri-BCP). Similarly, three main sets of peaks related to the distinctive α-CH (H_a @ 5.24 ppm) on pPDIV-*b*, and α-CH_2 protons (H_b @ 4.03 ppm and H_c @ 2.98 ppm) of the aliphatic chains from the respective blocks were observed. Integration of the aliphatic peaks (H_a, H_b and H_c corresponds to the formation of a tri-BCP (See SI Figure S5 for a detailed comparison between the ^{1}H NMR spectra of the macromonomers and tri-BCP). To further confirm the selectivity of the Heck reaction between the vinylene and halogen functional groups, two test reactions were performed using each macromonomer separately under Heck coupling conditions (See SI Figure S6). No increase in molecular weight consistent with macromonomer homocoupling was observed by SEC in either case confirming that both the terminal vinylene and bromo functionalities must be present to couple the macromonomers under the reaction conditions used.

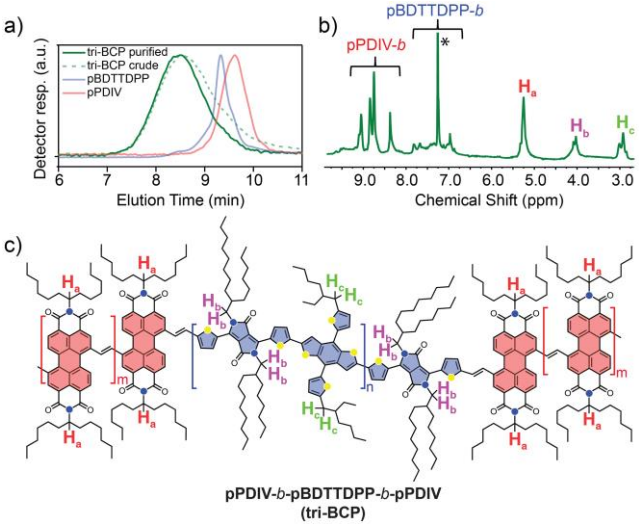

Figure 2. Characterization of tri-BCP (pPDIV-*b*-pBDTTDPP-*b*-pPDIV) (a) SEC traces consisting of tri-BCP (green solid trace), crude sample (green broken trace), pBDTTDPP (blue solid), and pPDIV (red solid). (b) ^{1}H NMR spectrum of tri-BCP and proton assignments on tri-BCP of the aromatic region and the respective protons on the aliphatic chains of the donor and acceptor blocks where * indicates chloroform solvent peak (See SI Figure S14 for the full ^{1}H NMR Spectrum). c) The chemical structure of tri-BCP with the protons of interest highlighted. Note that the S and N heteroatoms are colored yellow and blue, respectively.

Photophysical and electrochemical analysis were performed to further support the incorporation of both macromonomers in tri-BCP. The UV-Vis absorption spectrum of tri-BCP in chloroform shows two characteristic absorption peaks at λ_{max} = 748 nm and 638 nm that correspond to contributions from the donor pBDTTDPP-*b*, and acceptor pPDIV-*b* blocks, respectively (See SI Figure S7). The thin film spectrum of tri-BCP is similar to the solution spectrum, but red-shifted, as expected, due to the presence of intermolecular interactions in solid state. The photoluminescence (PL) emission spectrum of a tri-BCP thin film indicates a significant quenching (by 95%) of its emission peak at 709 nm (excitation at 633 nm) relative to a comparable amount of the acceptor macromonomer (See SI Figure S7c), and the quenching was improved compared to an analogous blend of the macromonomers. This suggests that the tri-BCP exhibits a superior photogenerated exciton separation efficiency, likely to due to proximity of the covalently linked donor and acceptor blocks. Cyclic voltammetry measurements of the tri-BCP (See SI Figure S8 and Table S4) yielded an estimated highest occupied molecular orbital (HOMO) of –5.39 eV (similar to that of the donor macromonomer), and a lowest unoccupied molecular orbital (LUMO) was estimated to be –3.89 eV, similar to that of the acceptor macromonomer (see Figure 3a, inset for energy level positions).

To evaluate the tri-BCP in SC-BHJ OPV devices and demonstrate the advantage of BCPs over polymer blend BHJs, inverted architecture devices (glass/In:SnO_2/ZnO/Active-Layer/MO_3/Ag) were fabricated and tested under standard 1 sun illumination (details of device fabrication and testing are described in the SI). For the active layer either the tri-BCP or a comparable blend of the macromonomers (molar ratio of 1:2 pBDTTDPP:pPDIV) were used. We note that the molar ratio and other device fabrication conditions were not optimized to maximize performance but used as a reasonable comparison to the tri-BCP. In addition, both blend and tri-BCP active layers had a similar thickness of ca. 120 nm as measured by profilometry. Current-density-voltage (*J-V*) curves of devices with the active layer as-cast from chloroform solution are shown in Figure S9, SI. The performance of these as-cast devices is relatively similar and poor with a PCE of 0.01% for tri-BCP and 0.04% for the blend. However, upon thermal annealing (150°C for 15 minutes) the performance between the two active layers became considerably different as shown in the *J-V* curves in Figure 3a. While the tri-BCP device improved significantly, achieving a short circuit current density J_{SC}, of over 6 mA cm^{-2} and reasonable PCE of 1.51%, the blend device decreased to 0.02%. A summary of the device performance parameters is presented in Table S5, SI, and the device external quantum efficiency (EQE) at short-circuit conditions is shown as a function of illumination wavelength and with respect to the UV-Vis absorbance of the macromonomers in Figure 3b. The difference in the EQE between the tri-BCP and the blend devices matches the *J-V* performance, and interestingly the EQE wavelength dependence of the tri-BCP corresponds well to the light absorption of both macromonomers, suggesting that light absorption by both components contributes to free charge generation.

To investigate a morphological explanation for the difference in device performance between the tri-BCP and the blend device, atomic force microscopy (AFM) images of the active layer were acquired (Figure 3c and 3d). Both as-cast films were relatively amorphous and smooth with a root-mean-square roughness of 1.17 nm and 1.14 nm, respectively, for the blend and tri-BCP (See inset images in Figure 3c and 3d). However, after thermal annealing, needle-like aggregates were observed in the blend film and the roughness

increased to 3.07 nm likely corresponding to the formation of crystalline domains due to large phase segregation of the donor and acceptor components. This is consistent with the decrease in photovoltaic performance of the blend devices after annealing. Conversely, tri-BCP showed a relatively amorphous morphology with small platelet sized and a slight increase in roughness to 1.55 nm after annealing (See Figure 3d). This indicates a stabilized donor-acceptor domain size where continued phase segregation under thermal stress is arrested by the covalent link between the components in the tri-BCP, as expected. While the device results presented here represent the proof-of-concept of our synthetic approach towards the preparation of functional donor:acceptor BCPs, we note that the further optimization of macromonomer lengths and molecular structure would be expected to yield significant increase in device PCE while retaining the thermal robustness compared to the polymer blend as demonstrated.

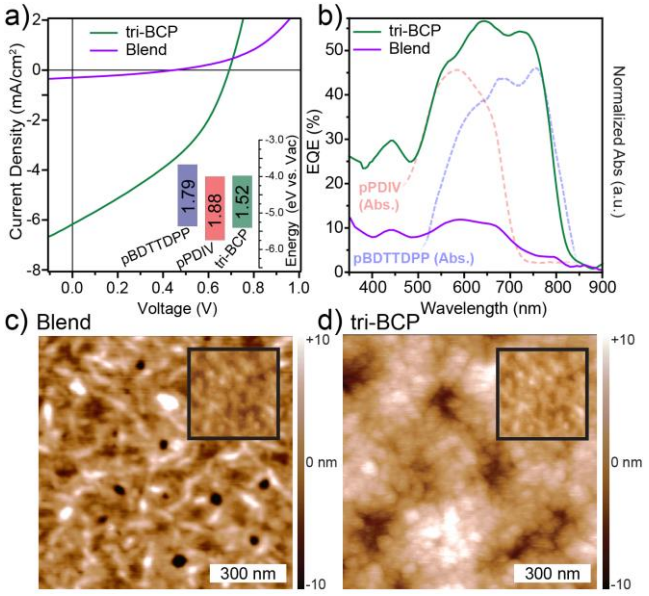

Figure 3. (a) Current density vs voltage curves of the OPV devices containing tri-BCP and a comparable macromonomer blend after thermal annealing at 150°C for 15 minutes. The inset shown the HOMO-LUMO gap energy positions; (b) The device EQE (solid lines) is shown in comparison to the UV-vis absorption of the macromonomers (broken lines). (c-d) morphological characterization by atomic force microscopy (height images) of the active layers after annealing at 150°C for 30 min (inset images are of the respective as-cast thin films).

In summary, we have demonstrated a new route to prepare fully-conjugated BCPs using a Heck-Mizoroki coupling between two functionalized macromonomers and without complications of end-group lability. The key to this route is the use of a vinylene monomer unit, which has a dual functionality as a planarizing bridging unit in the macromonomer backbone and as a functional end-group for the Heck coupling reaction. Precise end-group functionalities determined by MALDI-TOF MS were obtained for the pBDTTDPP-(Br/Br) donor and pPDIV-(H/V) acceptor macromonomers. Heck coupling resulted in a tri-BCP formation of pPDIV-*b*-pBDTTDPP-*b*-pPDIV configuration as evident from various chemical analysis. Photovoltaic performance of devices consisting of tri-BCP as the only light-absorbing component obtained a promising PCE of 1.51% after aggressive thermal annealing (150°C for 15 min), which was significantly larger than a comparable macromonomer blend (PCE of 0.02%). Morphological characterization suggested that the blend underwent large-scale phase segregation under annealing while the tri-BCP did not. This demonstrates the advantage of BCPs towards the fabrication of thermally robust OPVs. The further extension of our synthetic method towards other high-performance polymers systems, and the optimization of donor:acceptor ratio in the resulting BCPs is straightforward and will likely lead to advances in highly stable SC-BHJ OPVs with high PCE.

ASSOCIATED CONTENT

Supporting Information. Full details on material synthesis and experimental procedures as well as Figures S1-S9 and Tables S1-S5 as described in the main text. Additional NMR characterization of the monomers and the BCP (Figures S10-S14) is also included. This material is available free of charge via the Internet at http://pubs.acs.org

AUTHOR INFORMATION

Corresponding Author

* kevin.sivula@epfl.ch

Present Addresses

†Current address: Organic Materials Innovation Centre, School of Chemistry, University of Manchester, Oxford Rd, Manchester M13 9PL, United Kingdom

ACKNOWLEDGMENT

We thank the Swiss National Science Foundation (project number 200021_169215) for financial support of this work.

REFERENCES

1. Meng, L.; Zhang, Y.; Wan, X.; Li, C.; Zhang, X.; Wang, Y.; Ke, X.; Xiao, Z.; Ding, L.; Xia, R.; Yip, H.-L.; Cao, Y.; Chen, Y., Organic and Solution-Processed Tandem Solar Cells with 17.3% Efficiency. *Science* **2018,** *361,* 1094-1098.
2. Inganäs, O., Organic Photovoltaics over Three Decades. *Adv. Mater.* **2018,** *30,* 1800388.
3. Berny, S.; Blouin, N.; Distler, A.; Egelhaaf, H.-J.; Krompiec, M.; Lohr, A.; Lozman, O. R.; Morse, G. E.; Nanson, L.; Pron, A.; Sauermann, T.; Seidler, N.; Tierney, S.; Tiwana, P.; Wagner, M.; Wilson, H., Solar Trees: First Large-Scale Demonstration of Fully Solution Coated, Semitransparent, Flexible Organic Photovoltaic Modules. *Adv. Sci.* **2016,** *3,* 1500342.
4. Kang, H.; Kim, G.; Kim, J.; Kwon, S.; Kim, H.; Lee, K., Bulk-Heterojunction Organic Solar Cells: Five Core Technologies for Their Commercialization. *Adv. Mater.* **2016,** *28,* 7821-7861.
5. Zhang, Y.; Samuel, I. D. W.; Wang, T.; Lidzey, D. G., Current Status of Outdoor Lifetime Testing of Organic Photovoltaics. *Adv. Sci.* **2018,** *5,* 1800434.
6. Lee, H.; Park, C.; Sin, D. H.; Park, J. H.; Cho, K., Recent Advances in Morphology Optimization for Organic Photovoltaics. *Adv. Mater.* **2018,** *30,* 1800453.
7. Cheng, P.; Zhan, X., Stability of Organic Solar Cells: Challenges and Strategies. *Chem. Soc. Rev.* **2016,** *45,* 2544-2582.
8. Mitchell, V. D.; Jones, D. J., Advances Toward the Effective Use of Block Copolymers as Organic Photovoltaic Active Layers. *Poly. Chem.* **2018,** *9,* 795-814.
9. Johnson, K.; Huang, Y.-S.; Huettner, S.; Sommer, M.; Brinkmann, M.; Mulherin, R.; Niedzialek, D.; Beljonne, D.; Clark, J.; Huck, W. T. S.; Friend, R. H., Control of Intrachain Charge Transfer in Model Systems for Block Copolymer Photovoltaic Materials. *J. Am. Chem. Soc.* **2013,** *135,* 5074-5083.
10. Kuang, H.; Janik, M. J.; Gomez, E. D., Quantifying the Role of Interfacial Width on Intermolecular Charge Recombination in Block Copolymer Photovoltaics. *J. Polym. Sci., Part B: Polym. Phys.* **2015,** *53,* 1224-1230.
11. Grieco, C.; Aplan, M. P.; Rimshaw, A.; Lee, Y.; Le, T. P.; Zhang, W.; Wang, Q.; Milner, S. T.; Gomez, E. D.; Asbury, J. B., Molecular Rectification in

Conjugated Block Copolymer Photovoltaics. *J. Phys. Chem. C* **2016,** *120,* 6978-6988.
12. Smith, K. A.; Lin, Y.-H.; Mok, J. W.; Yager, K. G.; Strzalka, J.; Nie, W.; Mohite, A. D.; Verduzco, R., Molecular Origin of Photovoltaic Performance in Donor-block-Acceptor All-Conjugated Block Copolymers. *Macromolecules* **2015,** *48,* 8346-8353.
13. Guo, C.; Lee, Y.; Lin, Y.-H.; Strzalka, J.; Wang, C.; Hexemer, A.; Jaye, C.; Fischer, D. A.; Verduzco, R.; Wang, Q.; Gomez, E. D., Photovoltaic Performance of Block Copolymer Devices Is Independent of the Crystalline Texture in the Active Layer. *Macromolecules* **2016,** *49,* 4599-4608.
14. Nakabayashi, K.; Mori, H., All-Polymer Solar Cells Based on Fully Conjugated Block Copolymers Composed of Poly(3-hexylthiophene) and Poly(naphthalene bisimide) Segments. *Macromolecules* **2012,** *45,* 9618-9625.
15. Lee, Y.; Gomez, E. D., Challenges and Opportunities in the Development of Conjugated Block Copolymers for Photovoltaics. *Macromolecules* **2015,** *48,* 7385-7395.
16. Wang, S.; Yang, Q.; Tao, Y.; Guo, Y.; Yang, J.; Liu, Y.; Zhao, L.; Xie, Z.; Huang, W., Fully Conjugated Block Copolymers for Single-Component Solar Cells: Synthesis, Purification, and Characterization. *New J. Chem.* **2016,** *40,* 1825-1833.
17. Lombeck, F.; Komber, H.; Sepe, A.; Friend, R. H.; Sommer, M., Enhancing Phase Separation and Photovoltaic Performance of All-Conjugated Donor–Acceptor Block Copolymers with Semifluorinated Alkyl Side Chains. *Macromolecules* **2015,** *48,* 7851-7860.
18. Mok, J. W.; Lin, Y.-H.; Yager, K. G.; Mohite, A. D.; Nie, W.; Darling, S. B.; Lee, Y.; Gomez, E.; Gosztola, D.; Schaller, R. D.; Verduzco, R., Linking Group Influences Charge Separation and Recombination in All-Conjugated Block Copolymer Photovoltaics. *Adv. Funct. Mater.* **2015,** *25,* 5578-5585.
19. Guo, C.; Lin, Y.-H.; Witman, M. D.; Smith, K. A.; Wang, C.; Hexemer, A.; Strzalka, J.; Gomez, E. D.; Verduzco, R., Conjugated Block Copolymer Photovoltaics with near 3% Efficiency through Microphase Separation. *Nano Lett.* **2013,** *13,* 2957-2963.
20. Lee, Y.; Aplan, M. P.; Seibers, Z. D.; Kilbey, S. M.; Wang, Q.; Gomez, E. D., Tuning the Synthesis of Fully Conjugated Block Copolymers to Minimize Architectural Heterogeneity. *J. Mater. Chem. A* **2017,** *5,* 20412-20421.
21. Sommer, M.; Komber, H.; Huettner, S.; Mulherin, R.; Kohn, P.; Greenham, N. C.; Huck, W. T. S., Synthesis, Purification, and Characterization of Well-Defined All-Conjugated Diblock Copolymers PF8TBT-b-P3HT. *Macromolecules* **2012,** *45,* 4142-4151.
22. Verduzco, R.; Botiz, I.; Pickel, D. L.; Kilbey, S. M.; Hong, K.; Dimasi, E.; Darling, S. B., Polythiophene-block-polyfluorene and Polythiophene-block-poly(fluorene-co-benzothiadiazole): Insights into the Self-Assembly of All-Conjugated Block Copolymers. *Macromolecules* **2011,** *44,* 530-539.
23. Ku, S.-Y.; Brady, M. A.; Treat, N. D.; Cochran, J. E.; Robb, M. J.; Kramer, E. J.; Chabinyc, M. L.; Hawker, C. J., A Modular Strategy for Fully Conjugated Donor–Acceptor Block Copolymers. *J. Am. Chem. Soc.* **2012,** *134,* 16040-16046.
24. Nübling, F.; Komber, H.; Sommer, M., All-Conjugated, All-Crystalline Donor–Acceptor Block Copolymers P3HT-b-PNDIT$_2$ via Direct Arylation Polycondensation. *Macromolecules* **2017,** *50,* 1909-1918.
25. Senkovskyy, V.; Tkachov, R.; Komber, H.; Sommer, M.; Heuken, M.; Voit, B.; Huck, W. T. S.; Kataev, V.; Petr, A.; Kiriy, A., Chain-Growth Polymerization of Unusual Anion-Radical Monomers Based on Naphthalene Diimide: A New Route to Well-Defined n-Type Conjugated Copolymers. *J. Am. Chem. Soc.* **2011,** *133,* 19966-19970.
26. Benten, H.; Mori, D.; Ohkita, H.; Ito, S., Recent research progress of polymer donor/polymer acceptor blend solar cells. *J. Mater. Chem. A* **2016,** *4,* 5340-5365.
27. Zhang, S.; Ye, L.; Hou, J., Breaking the 10% Efficiency Barrier in Organic Photovoltaics: Morphology and Device Optimization of Well-Known PBDTTT Polymers. *Adv. Energy Mater.* **2016,** *6,* 1502529.
28. Po, R.; Bianchi, G.; Carbonera, C.; Pellegrino, A., "All That Glisters Is Not Gold": An Analysis of the Synthetic Complexity of Efficient Polymer Donors for Polymer Solar Cells. *Macromolecules* **2015,** *48,* 453-461.
29. Grisorio, R.; Suranna, G. P., Intramolecular Catalyst Transfer Polymerisation of Conjugated Monomers: From Lessons Learned to Future Challenges. *Poly. Chem.* **2015,** *6,* 7781-7795.
30. Morin, P.-O.; Bura, T.; Leclerc, M., Realizing the Full Potential of Conjugated Polymers: Innovation in Polymer Synthesis. *Mater. Horizons* **2015.**
31. Wang, J.; Higashihara, T., Synthesis of All-Conjugated Donor-Acceptor Block Copolymers and Their Application in All-Polymer Solar Cells. *Poly. Chem.* **2013,** *4,* 5518-5526.
32. Nübling, F.; Yang, D.; Müller-Buschbaum, P.; Brinkmann, M.; Sommer, M., In Situ Synthesis of Ternary Block Copolymer/Homopolymer Blends for Organic Photovoltaics. *ACS Appl. Mater. Interfaces* **2018,** *10,* 18149-18160.
33. Lee, D. H.; Lee, J. H.; Kim, H. J.; Choi, S.; Park, G. E.; Cho, M. J.; Choi, D. H., $(D)_n$-σ-$(A)_m$ Type Partially Conjugated Block Copolymer and its Performance in Single-Component Polymer Solar Cells. *J. Mater. Chem. A* **2017,** *5,* 9745-9751.
34. Lee, J. H.; Park, C. G.; Kim, A.; Kim, H. J.; Kim, Y.; Park, S.; Cho, M. J.; Choi, D. H., High-Performance Polymer Solar Cell with Single Active Material of Fully Conjugated Block Copolymer Composed of Wide-Band gap Donor and Narrow-Band gap Acceptor Blocks. *ACS Appl. Mater. Interfaces* **2018,** *10,* 18974-18983.
35. Gasperini, A.; Johnson, M.; Jeanbourquin, X.; Yao, L.; Rahmanudin, A.; Guijarro, N.; Sivula, K., Semiconducting Alternating Multi-Block Copolymers via a Di-Functionalized Macromonomer Approach. *Poly. Chem.* **2017,** *8,* 824-827.
36. Koldemir, U.; Puniredd, S. R.; Wagner, M.; Tongay, S.; McCarley, T. D.; Kamenov, G. D.; Müllen, K.; Pisula, W.; Reynolds, J. R., End Capping Does Matter: Enhanced Order and Charge Transport in Conjugated Donor–Acceptor Polymers. *Macromolecules* **2015,** *48,* 6369-6377.
37. Yokozawa, T.; Ohta, Y., Transformation of Step-Growth Polymerization into Living Chain-Growth Polymerization. *Chem. Rev.* **2016,** *116,* 1950-1968.
38. Gu, C.; Li, Y.; Xiao, L.; Fu, H.; Wang, D.; Cheng, L.; Liu, L., Tunable Heck–Mizoroki Reaction of Dibromonaphthalene Diimide with Aryl Ethylenes: Design, Synthesis, and Characterization of Coplanar NDI-Based Conjugated Molecules. *J. Org. Chem.* **2017,** *82,* 12806-12812.
39. Guo, Y.; Li, Y.; Awartani, O.; Zhao, J.; Han, H.; Ade, H.; Zhao, D.; Yan, H., A Vinylene-Bridged Perylenediimide-Based Polymeric Acceptor Enabling Efficient All-Polymer Solar Cells Processed under Ambient Conditions. *Adv. Mater.* **2016,** *28,* 8483-8489.
40. Fei, Z.; Han, Y.; Martin, J.; Scholes, F. H.; Al-Hashimi, M.; AlQaradawi, S. Y.; Stingelin, N.; Anthopoulos, T. D.; Heeney, M., Conjugated Copolymers of Vinylene Flanked Naphthalene Diimide. *Macromolecules* **2016,** *49,* 6384-6393.
41. Zhang, L.; Rose, B. D.; Liu, Y.; Nahid, M. M.; Gann, E.; Ly, J.; Zhao, W.; Rosa, S. J.; Russell, T. P.; Facchetti, A.; McNeill, C. R.; Brédas, J.-L.; Briseno, A. L., Efficient Naphthalenediimide-Based Hole Semiconducting Polymer with Vinylene Linkers between Donor and Acceptor Units. *Chem. Mater.* **2016**, *28,* 8580–8590.
42. Dou, L.; You, J.; Yang, J.; Chen, C.-C.; He, Y.; Murase, S.; Moriarty, T.; Emery, K.; Li, G.; Yang, Y., Tandem Polymer Solar Cells Featuring a Spectrally Matched Low-Bandgap Polymer. *Nat. Photon.* **2012,** *6,* 180-185.
43. Ma, Y.; Wu, Y.; Zhao, Y.; Fu, H.; Yao, J., Synthesis and Photophysics of Monodisperse Co-Oligomers Consisting of Alternating Thiophene and Perylene Bisimide. *Phys. Chem. Chem. Phys.* **2011,** *13,* 2036-2043.
44. Wen, S.; Chen, W.; Fan, M.; Duan, L.; Qiu, M.; Sun, M.; Han, L.; Yang, R., A Diketopyrrolopyrrole-Based Low Bandgap Polymer with Enhanced Photovoltaic Performances through Backbone Twisting. *J. Mater. Chem. A* **2016,** *4,* 18174-18180.
45. Zhou, Y.; Yan, Q.; Zheng, Y.-Q.; Wang, J.-Y.; Zhao, D.; Pei, J., New Polymer Acceptors for Organic Solar Cells: The Effect of Regio-Regularity and Device Configuration. *J. Mater. Chem. A* **2013,** *1,* 6609-6613.
46. Goto, E.; Ando, S.; Ueda, M.; Higashihara, T., Nonstoichiometric Stille Coupling Polycondensation for Synthesizing Naphthalene-Diimide-Based π-Conjugated Polymers. *ACS Macro Lett.* **2015,** *4,* 1004-1007.

Insert Table of Contents artwork here

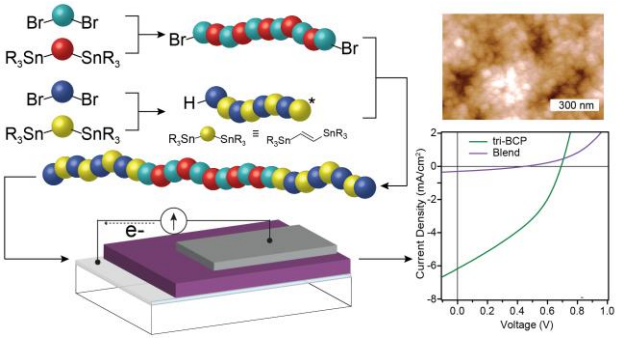

Supporting Information

Fully-Conjugated Donor-Acceptor Block-Copolymers for Organic Photovoltaics via Heck-Mizoroki Coupling

Aiman Rahmanudin,† Liang Yao, Arvindh Sekar, Han-Hee Cho, Yongpeng Liu, Charles R. Lhermitte and Kevin Sivula*

Laboratory for Molecular Engineering of Optoelectronic Nanomaterials, École polytechnique fédérale de Lausanne (EPFL), Station 6, CH-1015, Switzerland

*Email: kevin.sivula@epfl.ch

Contents:

General Experimental Procedures

Thin Film Preparation, device fabrication and characterization:

Solution preparation of macromonomers, tri-BCP and its molar blend

Each respective material was prepared by first dissolving each stock solution separately for 12hrs at 50°C in chloroform (CF) at a concentration of 20mg/ml, before filtering with a 1.0µm pore diameter PTFE filter, and left to stir for another hour before deposition onto the respective substrates. For the blend solution, each component was mixed and left to stir for at least 2hrs before filtering.

Spin coated thin film preparation

Pre-patterned ITO on glass was cleaned by sequential sonication in water, isopropanol and acetone for 30 min each, and dried by argon. ZnO (20 nm) was utilized for the electron transport layer in the inverted solar cells. The ZnO precursor solution, which contains 0.5 M zinc acetate dehydrate and 0.5 M monoethanolamine in 2-methoxyethanol, was stirred under 60 °C for overnight. The ZnO electron transport layer was deposited on the clean ITO substrates via spin-coating with the spin rate of 5000 rpm. After exposing a section of the ITO electrical contact, the substrates were annealed at 200 °C in air for 30 min to obtain a thin layer of ZnO film on ITO. The respective solution prepared were then prepared via spin-coating onto the substrate at 1500rpm for 60 seconds to obtain a thickness of approximately ≈120nm as measured from a Bruker Dektak XT profilometer.

UV-Vis and PL Characterization:

Absorption spectra of the solution and thin films were acquired with a UV–vis-NIR UV-3600 (Shimadzu) spectrophotometer, and the optical band gap (E_g^{opt}) was determined from the absorption edge of the thin film sample. Photoluminescence spectra of the thin films were carried out on a Fluorolog-3

spectrofluorometer (Horiba) equipped with a Xe lamp with an excitation light source at 532 nm. The sample was placed at a 45° from the lamp to the detector.

Cyclic voltammetry measurements: The electrochemical CV was conducted on a computer controlled SP-200 potentiostat (Biologic Technologies) in a three electrode configuration with a glassy carbon disk, Pt wire and Ag/Ag^+ electrode as the working electrode, counter electrode, and reference electrode, respectively in a 0.1 M tetrabutylammonium hexafluorophosphate (Bu_4NPF_6) acetonitrile solution as supporting electrolyte, at a scan rate of 50mV s^{-1}. Thin Films of individual primary component were drop casted on a bare Pt foil from a 2.0mgmL^{-1} CF solution. The potential of Ag/Ag^+ reference electrode was internally calibrated by using Ferrocene/Ferrocenium (Fc/Fc^+) redox couple. The electrochemical energy levels were estimated by using the empirical formula: E_{HOMO}= −(4.80 + $E_{onset,\ ox}$) and E_{LUMO}= −(4.80 + $E_{onset,\ red}$). A platinum bead was used as a working electrode, a platinum wire was used as an auxiliary electrode, and a silver wire was used as a pseudo-reference. Fc/Fc^+ was used as an internal standard, and potentials were recorded versus $FeCp_2^+$ /$FeCp_2^0$.

Solar-Cell Fabrication and Testing

Upon spin coating of the respective BHJ active layer on ZnO/ITO/Glass, the substrates were then transferred into the deposition chamber to thermally evaporate 4 nm of MoO_3 and 100 nm Ag at ~10^{-6} mbar through a shadow mask with an active area of 16 mm^2 by thermal evaporation (Kurt J. Lesker Mini-SPECTROS). Electronic characterization was performed under simulated AM1.5G irradiation from a 300 W Xe arc lamp set to 100 mW cm^{-2} with a calibrated Si photodiode (ThorLabs) at room temperature. Current–voltage curves were obtained with a Keithley 2400 source measure unit. Thermal annealing at 150°C for 15 minutes was performed after the deposition of the top electrode under argon atmosphere and cooled down to room temperature before measuring its photovoltaic performance. Electronic characterization was measured by Keithley 2400 source measure unit. The external quantum efficiency (EQE) of the devices was characterized by illumination from a Tunable PowerArc illuminator (Optical Building Blocks Corporation). A calibrated Si photodiode was employed to measure the incident photon number at each wavelength.

General synthetic/characterization procedures

Analytical Size exclusion Chromatography (SEC) and Preparatory-SEC (prep-SEC):

Polymers were analyzed and fractionalized using Shimadzu Prominence LC-20AP (Preparative Liquid Chromatography) in chlorobenzene solvent at 80°C with the UV-Vis detectors at 663 nm and 552 nm. Preparative size exclusion chromatography was performed by firstly dissolving 100 mg of product dissolved in 10 ml of chlorobenzene (80°C) and injecting the solution in a size exclusion preparative column (PSS SDV preparative linear M, 40mm×250mm) at 80°C using chlorobenzene as mobile phase at a constant elution flow of 6 mL/min. Fraction collection was carried out every 20 seconds (0.33 mL). Single fractions (and crude polymerizations) were analyzed through an analytical size exclusion PSS SDV analytical linear M column (8 mm × 250 mm, 80°C, CB mobile phase, 1 mL/min).

Matrix assisted laser desorption/ionization time-of-flight Mass spectrometry (MALDI-TOF MS)

Separate solution of the matrix (trans-2-[3-(4-tert-Butylphenyl)-2-methyl-2-propenyllidene] malononitrile) at 5 mg/mL in tetrahydrofuran (THF), and the respective polymer at 5 mg/mL in CF were mixed at a ratio of 2:1 – matrix:polymer, where a volume of 1µL of the mixture was dropped on the target and allowed to dry at room temperature before measurements. Mass spectra were acquired in the positive-ion reflector mode at the respective detection range.

^{1}H Nuclear Magnetic Resonance (^{1}H NMR)

For monomer characterization: The (^{1}H) & (^{13}C) NMR spectra were recorded at room temperature using per-deuterated solvents as internal standards on a 400 MHz NMR Bruker AVANCE III-400 spectrometer (Bruker, Rheinstetten, Germany) unless explicitly mentioned. Macromonomer and tri-BCP characterization were performed on a 800 MHz NMR Bruker AVANCEII-800 spectrometer (Bruker, Rheinstetten, Germany). Chemical shifts are given in parts per million (ppm) referenced to residual ^{1}H or ^{13}C signals in deuterated chloroform- *d*, and tetrachloroethane-d_2.

General Synthetic methods:

All reagents were of commercial reagent grade (Sigma-Aldrich, Acros & Fluorochem) and were used without further purification. Toluene, CF, THF (Fisher Chemical, HPLC grade) and chlorobenzene (Alfa Aesar, HPLC grade) were purified and dried on a Pure Solv-MD Solvent Purification System (Innovative Technology, Amesbury, United States) apparatus. Normal phase silica gel chromatography was performed with an Acros Organic silicon dioxide (pore size 60 Å, 40–50 µm technical grades). EI-MS spectrum was recorded on an EI/CI-1200L GC-MS (Varian) instrument & APPI-MS spectrum was recorded on an ESI/APCI LC-MS Autopurification System with a ZQ Mass detector (Waters, Milford, United States) instrument using a positive mode.

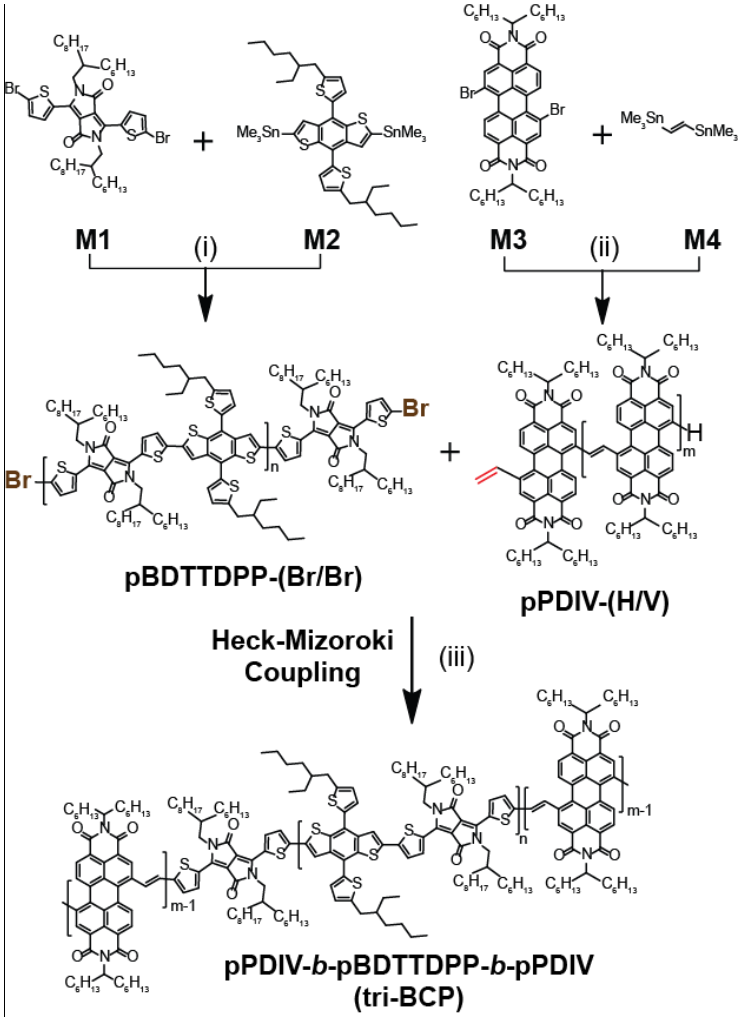

Scheme S1. Full synthetic route for the formation of tri-BCP, pPDIV-*b*-pBDTTDPP-*b*-pPDIV.

Macromonomer Synthesis Procedures

Synthesis of pBDTTDPP-(Br/Br)

In an over-dried Schlenck tube, the monomers M1 and M2 were added at the specified molar ratios, and the reagents were dried under vacuum and flushed with argon (3x). The tube was then transferred into an argon glove box, to add $Pd(PPh_3)_4$ at a 10% molar equivalence. This mixture was then dissolved in Toluene:DMF at a volume ratio of 10:1 ratio with a concentration of concentration 0.76 mg/mL of the total mass of the starting monomers. After removal from the glove box, the solution was degassed with an argon-vacuum evacuation cycle (3x), and subsequently heated at 95°C for 12 h. To stop the reaction, the mixture was cooled to room temperature and a 2M solution of potassium fluoride was added and left to stir for an hour before precipitation in excess methanol. The solid precipitate was then filtered over celite, and washed with three rounds of methanol and hexane. The crude mixture was then dissolved in CF and subjected to GPC analysis before performing prep-SEC, and an average reaction yield 46% was obtained. After purification, the polymer was characterized *via* ^{1}H NMR, MALDI TOF MS and SEC as described in the main text.

Synthesis of pPDIV-(H/V)

In an over-dried schlenck tube, the monomers M3 and M4 were added at the specified molar ratios, and the tube was transferred into an argon glove box. Pd_2dba_3 and P(o-tol)$_3$ at 5% and 20% molar equivalence (ratio of 1:4) was added into the tube, and the solid mixture was dissolved in toluene at a concentration of 37.5 mg/mL of the total mass of the monomers. After removal from the glove box, the solution was degassed with an argon-vacuum evacuation cycle (3x), and subsequently heated at 95°C for 12 h. To stop the reaction, the mixture was cooled to room temperature and a solution of 2M HCl was added and left to stir for an hour before precipitation in excess methanol. The solid precipitate was then filtered over celite, and washed with three rounds of methanol and hexane. The crude mixture was then dissolved in CF and subjected to GPC analysis before performing prep-SEC, and an average reaction yield 96% was obtained. After purification, the polymer was characterized *via* ^{1}H NMR, MALDI TOF MS and SEC as described in the main text.

Tri-BCP Synthesis Procedure

The respective marcomonomers were added into a 10 ml Schlenk flask at a stoichiometric ratio of 1:2.3 - **pBDTTDPP-(Br/Br)**: **pPDIV-(H/V)**, and dissolved in a mixture of Tol:DMF: triethylamine (TEA) – 0.3 : 0.3: 0.25 at a concentration of 20 mg/mL with respective to the total weight ratio of the macromonomers. $Pd(OAc)_2$ (5% mol) and P-(*o*-tol)$_3$ (20%mol) was then added into the reaction solution. The flask was subsequently degassed and purged with Argon (3 cycles), and was left at 95°C for 12 h. After cooling the crude reaction to room temperature, methanol was added into flask to precipitate crude polymer. This was then filtered through celite and washed with methanol and hexane sequentially, and finally dissolved in CF which was evaporated and precipitated in methanol to collect a solid crude product. The crude was then purified *via* prep-SEC to obtain the purified sample of tri-BCP. After purification, the polymer was characterized *via* ^{1}H NMR, and analytical SEC as described in the main text.

Monomer Synthesis Procedures and Characterization

M1 and M2 were synthesized according literature procedure[S1] and the precursor (C_6H_{13})PDI for M3 was synthesized according to literature procedure.[S2] M4 was purchased commercially from Sigma Aldrich and used without further purification.

Synthesis of M3

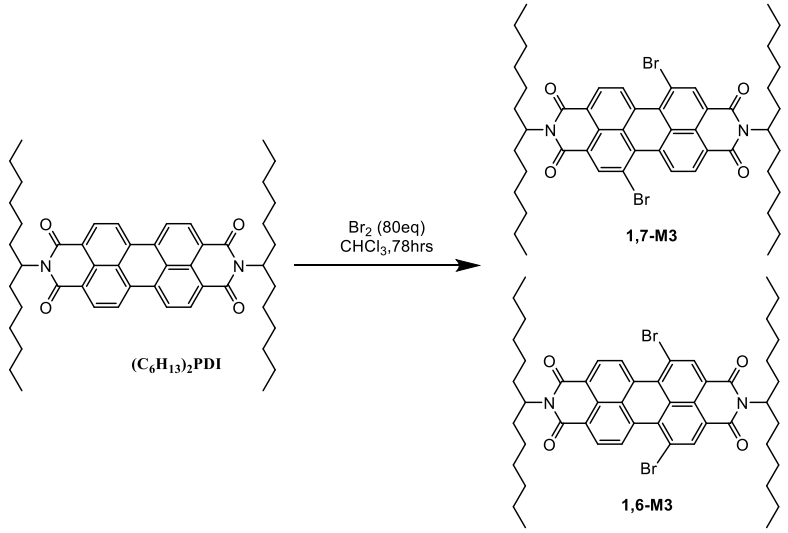

(C_6H_{13})$_2$PDI (1.00 gm; 1.32 mmol; 1 eq.) was taken in a Schlenk flask and dissolved in CF (10 mg/mL concentration). Then, argon gas was bubbled through for 10 minutes to remove dissolved gases. Excess liquid bromine (5.5 mL; 80eq.) was injected into the solution and the flask was heated to reflux for 72 h. After cooling down the solution, compressed air was bubbled to remove bromine (channeled into reducing agent). The crude was adsorbed onto dry silica to perform dry loaded column chromatography. Broadly, three fractions were isolated and the fraction with the highest R_f value is mixture of the two 1,6 and 1,7 M3 isomers. Flash column chromatography using an elution of CF/Hexane were performed to isolate out the mono brominated PDI and any unreacted starting compound. The separated mixture of M3 isomers was then recrystallized by heating in solvent mixture of isoprpanol:hexane at 70°C until the solid dissolves and left to cool overnight. The crystals formed were filtered, redissolved and cooled down multiple times until the purity of the crystals obtained reaches approximately 97% at a ratio of 1:42 (1,6-M3:1,7-M3) as confirmed by ^{1}H NMR (See Figure S2).

^{1}H NMR (800 MHz, Chloroform-*d* at 50°C) δ 9.67 (d, *J* = 7.8 Hz, 1H), 9.08 (s, 1H), 9.00 – 8.76 (m, 1H), 5.34 (tt, *J* = 9.9, 5.9 Hz, 1H), 2.41 (dtd, *J* = 14.6, 9.6, 5.1 Hz, 3H), 2.03 (ddt, *J* = 15.0, 10.8, 5.2 Hz, 3H), 1.45 (dddd, *J* = 58.4, 21.4, 14.5, 6.8 Hz, 21H), 1.01 (t, *J* = 7.0 Hz, 6H); MS APCI (positive mode): 913.296 m/z. See Figures S10 and S11 for NMR characterization.

Supporting Figures and Tables

Table S1. Summary of reported PCE of SC-BCP and its respective synthetic methodology

Entry	SC-BCP[c]	Method	M_n (kg mol^{-1})	J_{sc} (mA/cm^{-2})	V_{oc} (V)	Fill Factor (%)	PCE (%)	Ref.
1	P3HT-*b*-PFTBT	1. Grignard metathesis (GRIM) Polymerization 2. Suzuki Coupling	35.8	3.1	1.10	26	0.91	17
2	P3HT-F-PFTBT	Same as above	29.0	4.73	1.11	42	2.24	18
3	P3HT-*b*-PFTBT	Same as above	29.0	5.2	1.23	47	2.7	19
4[a]	P3HT-PNBI-P3HT	1. GRIM and Stille polymerization 2. Yamamoto Coupling	21.8	4.57	0.56	39	1.28	9
5	P3HT-*b*-PBIT2	1. GRIM 2. Stille Polymerization	25.2	5.29	0.43	43	1.00	14
6[b]	PTQI-*b*-PNDIS	1. Stille Polymerization 2.Stille Coupling	12.4	4.04	0.79	48.1	1.54	33
7	P3	1. Stille Polymerization 2.Stille Coupling	18.3	8.26	0.86	50.3	3.87	34
8	tri-BCP	1. Stille polymerization 2. **Heck-Mizoroki Coupling**	16.9	6.17	0.72	40	1.51	**This work***

[a] GRIM polymerization was used for the P3HT macroinitiator while Stille coupling was used to prepare the acceptor monomer before the final Yamamoto coupling to obtain P3HT-PNBI-P3HT.
[b] Individual donor and acceptor block were prepared via Stille polymerization and Stille coupling was used for the BCP reaction.
[c] See structures below

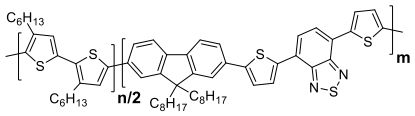

1 and 2 - P3HT-*b*-PFTBT

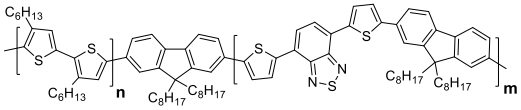

3 - P3HT-*F*-PFTBT

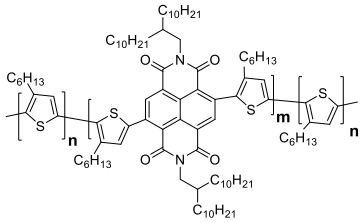

4 - P3HT-PNBI-P3HT

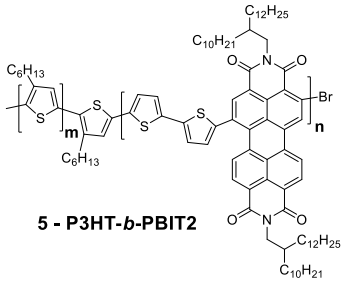

5 - P3HT-*b*-PBIT2

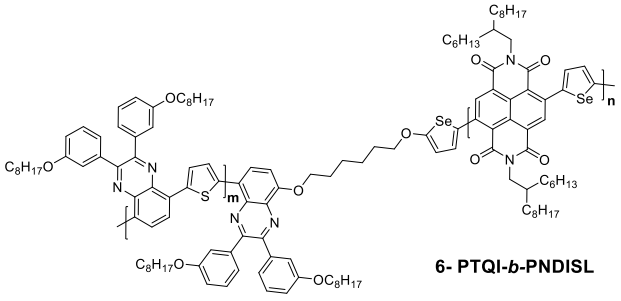

6- PTQI-*b*-PNDISL

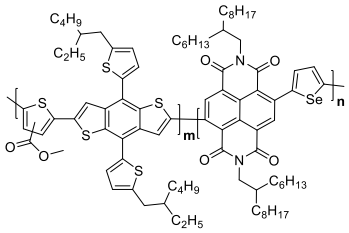

7- P3

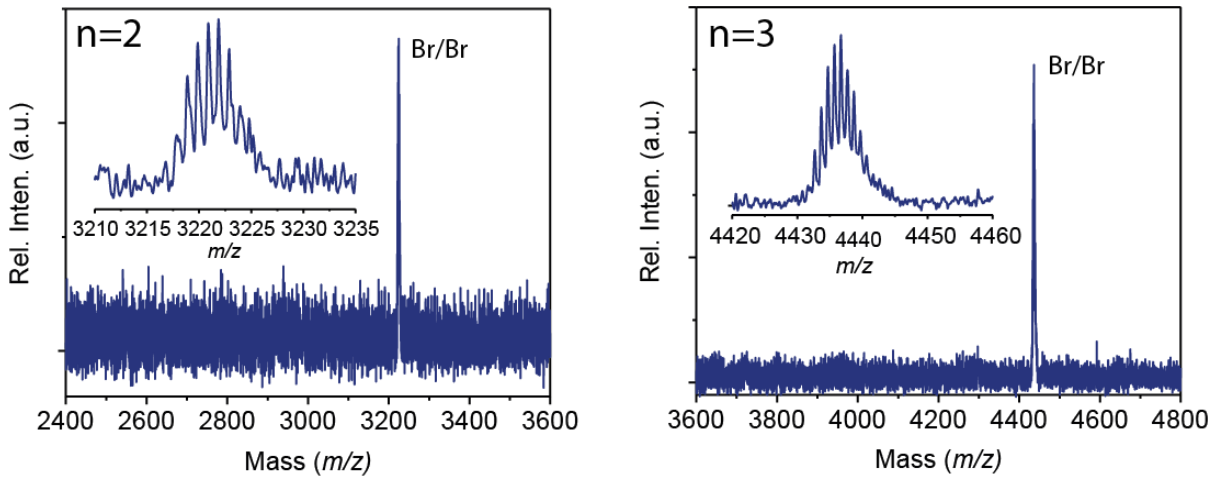

Figure S1. Representative mass spectrum of pBDTTDPP-(Br/Br) magnified at the peaks for n=2 (left panel) and n=3 (right panel). Insets are a further magnification of the peaks.

Table S2. Representative summary of estimated and calculated m/*z* of pBDTTDPP-(Br/Br) at m=3 and 4.

End capping groups	m	Calculated	[a]Experimental
H/Br	3	2509.9	-
	4	3724.9	-
Br/Br	3	3224.79	3220.39
	4	4439.79	4436.88

[a] Values were assigned from the highest peak on the MALDI-TOF spectrum shown in Figure S1.

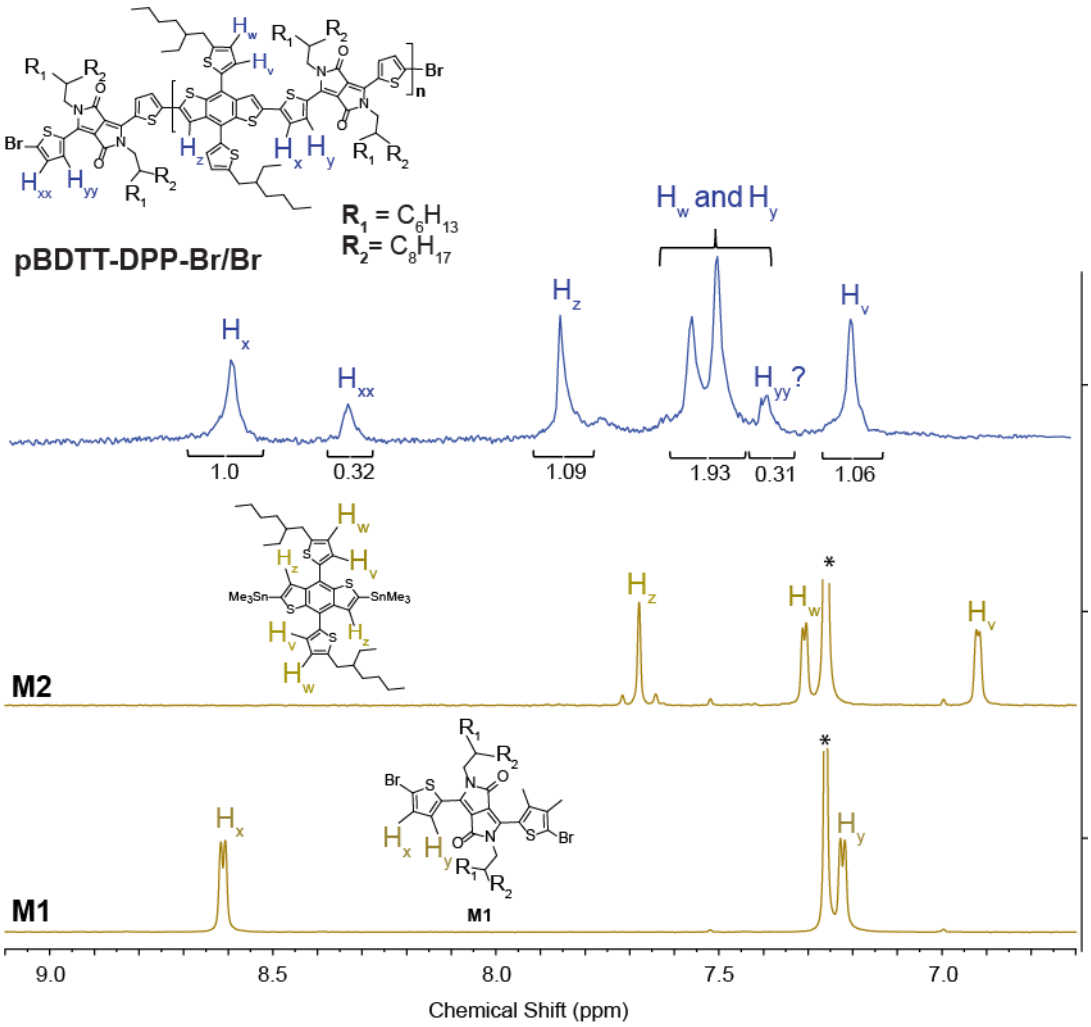

Figure S2. Zoomed 800 Mhz ^{1}H NMR spectrum of pBDTTDPP-(Br/Br) stacked with the corresponding monomer M2 and M1 to indicate the relation of the respective protons or the aromatic region in the marcomonomer. Full ^{1}H NMR spectrum of pBDTTDPP-(Br/Br) is shown in the experimental procedure figure S10 (*indicates deuterated chloroform peak for M1 and M2, while deuterated tetrachloroethane was used for PBDTT-DPP-Br_2 not shown in the NMR spectrum – 6.0ppm).

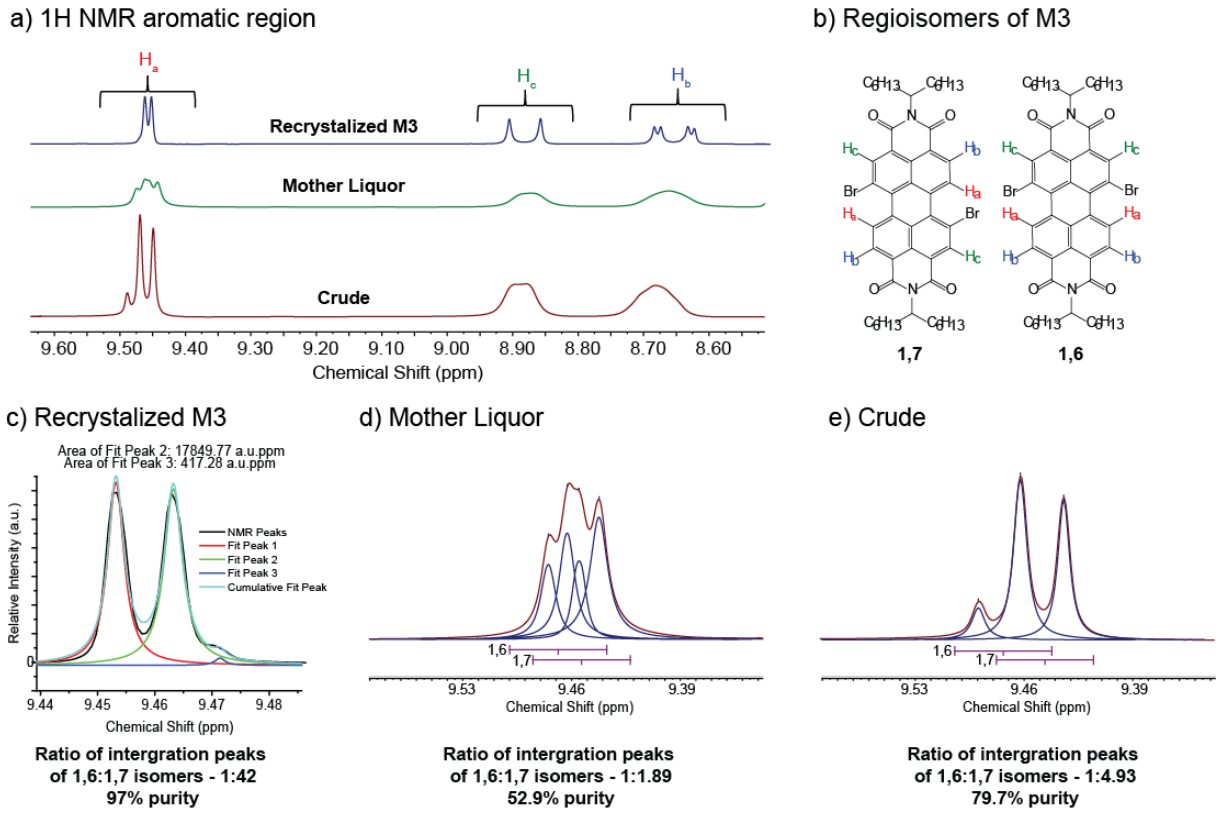

Figure S3. 800 Mhz ^{1}H NMR analysis of the monomer M3. a) ^{1}H NMR spectrum of the aromatic region of the crude, recrystallized and mother liquor samples of M3; b) Schematic of the 1,6 and 1,7 regio-isomers of M3; c) Calculation of the integration peaks of proton environment, H_a , to determine the purity of the 1,7 isomer (Deconvolution assuming a Lorentzian behavior of the peaks for recrystallization of M3 had to be performed in origin since the integration of the 1,6 peak was not detected in MestReNova, unlike the mother liquor and crude samples). The aromatic region of the recrystallization mother liquor and the crude (non-recrystallized) material is also shown in (d) and (e), respectively, for comparison. Refer to Figure S10 and S11 below for proton assignments of M3 via ^{1}H NMR and 2D-COSY spectroscopy.

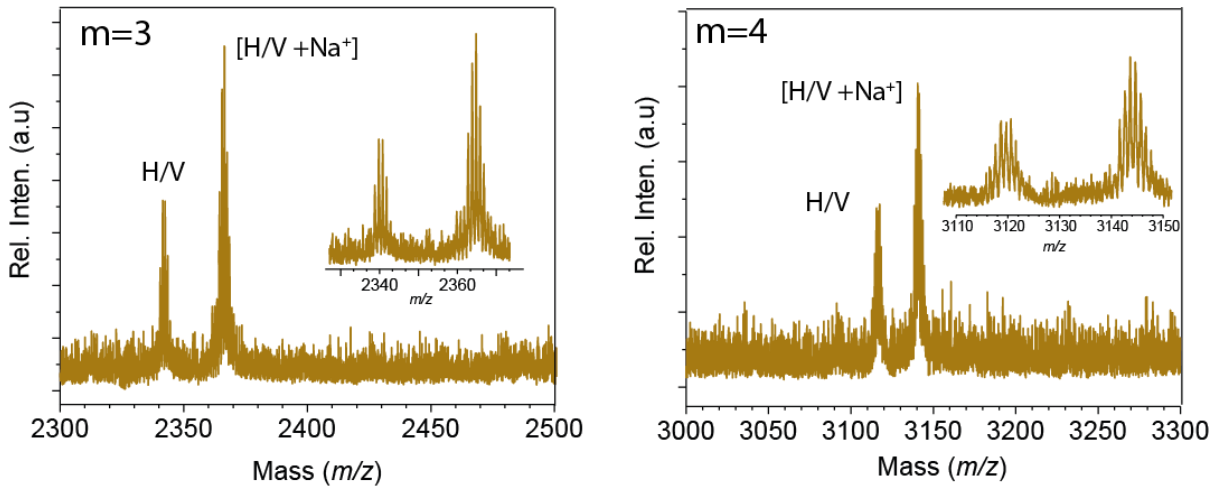

Figure S4. Representative mass spectrum of pPDIV-(H/V) magnified at the peaks for m=3 and 4. Insets are a further magnification of the peaks.

Table S3. Representative summary of estimated and calculated m/*z* of pPDIV at m=3 and 4.

End capping groups	m	Calculated		[a]Experimental	
		(M)	(M+Na$^+$)	(M)	(M+Na$^+$)
H/H	3	2316.33	2339.33	-	-
	4	3097.44	3120.44	-	-
H/V	3	2343.33	2366.33	2342.46	2365.28
	4	3124.44	3147.44	3123.42	3146.75
V/V	3	2370.38	2393.38	-	-
	4	3151.49	3174.49	-	-
Br/V	3	2444.33	2467.33	-	-
	4	3225.44	3248.44	-	-

[a] Values were assigned from the highest peak on the MALDI-TOF spectrum shown in Figure S4.

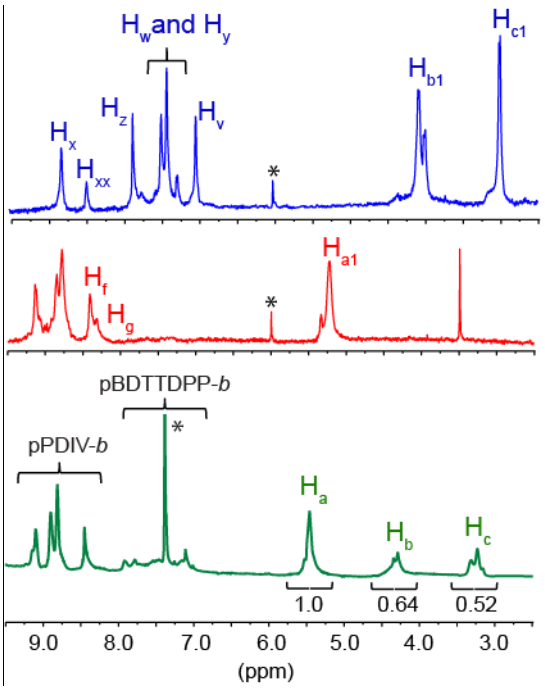

Figure S5. 800 Mhz ^{1}H NMR spectra of the macromonomers and tri-BCP zoomed to the chemical shift to indicate the aromatic region and the distinctive aliphatic protons (H_a, H_b and H_c). (*)indicates deuterated tetrachloroethane peak for pBDTTDPP-(Br/Br) and pPDIV-(H/V) and deuterated chloroform for tri-BCP, and Full ^{1}H NMR spectra of pBDTTDPP-(Br/Br), pPDIV-(H/V) and tri-BCP are shown in the experimental procedure Figure S10, S11 and S12.

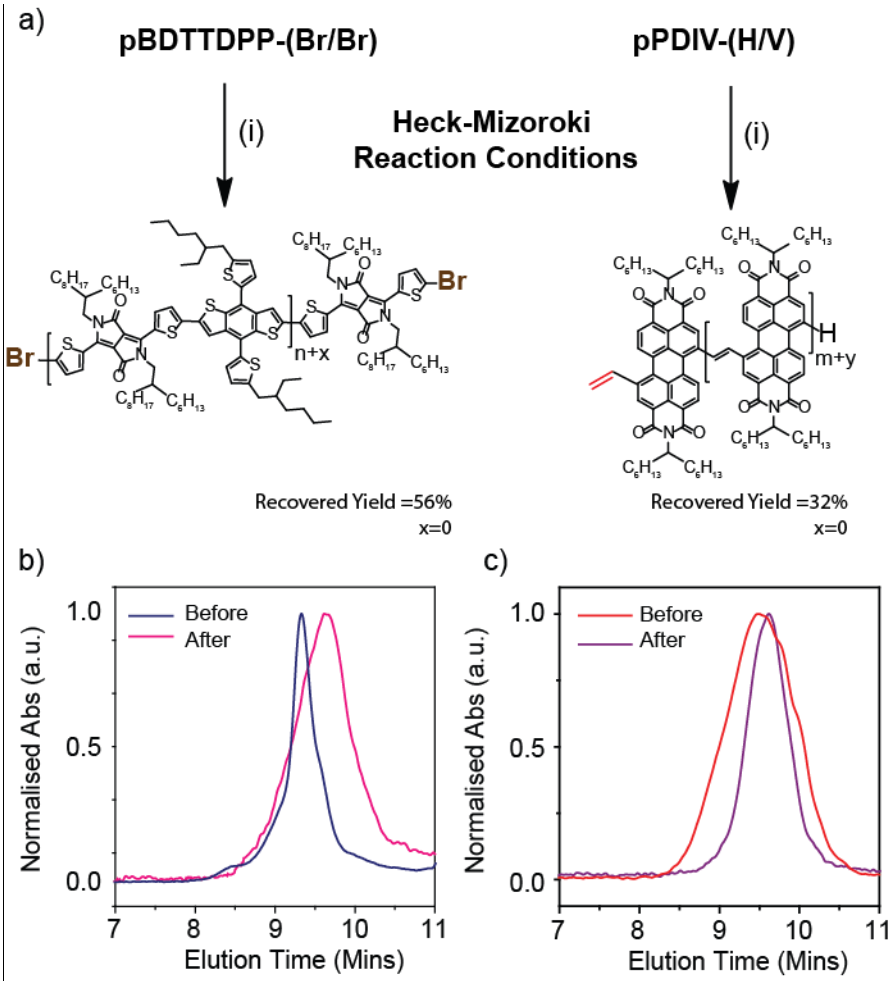

Figure S6. a) Reaction scheme of homopolymer test reaction under Heck-Mizoroki coupling conditions: (i) pBDTT-DPP-Br_2 or pPDIV-(H/V) (1eq), $Pd(OAc)_2$ (5%), P-(o-tol)$_3$ (20%), TEA:DMF:Toluene, 95°C, 12h; GPC traces of the reaction before and after b) pBDTTDPP-(Br/Br) (M_n = 3.68 kg mol^{-1}, $Đ$=1.45 and recovered yield =55%); c) pPDIV-(H/V) (M_n = 3.52 kg mol^{-1}, $Đ$=1.32 and recovered yield =32%);. The reaction was performed using the procedure described for the synthesis of tri-BCP and the GPC analysis were measured after work-up and without purification using prep-SEC.

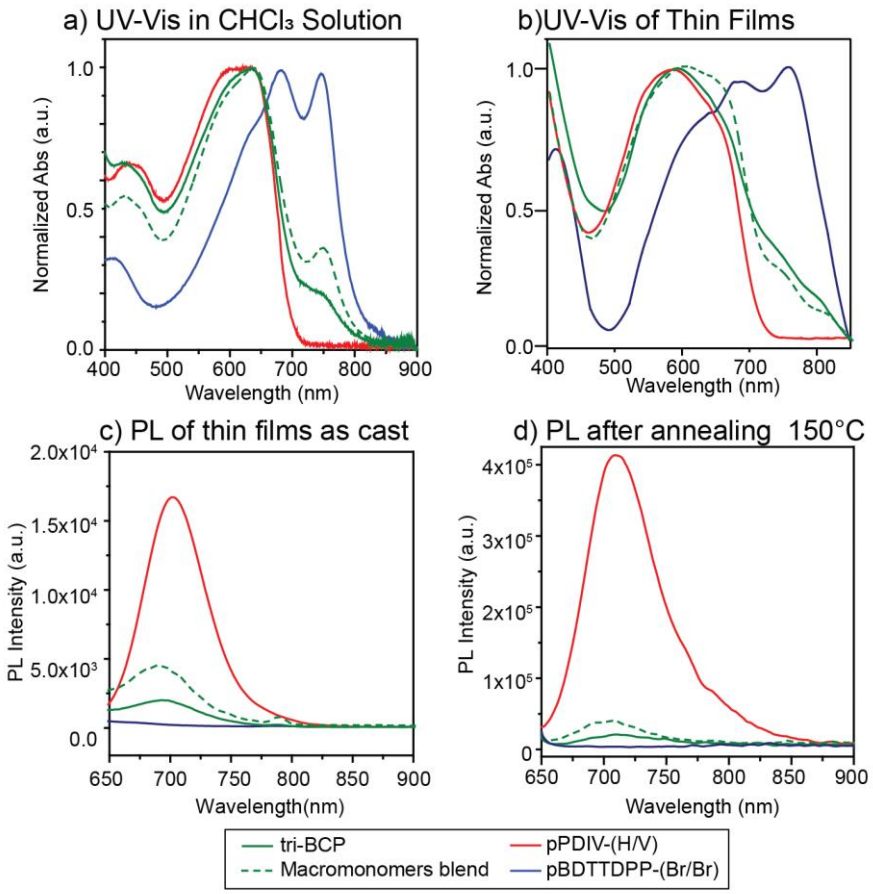

Figure S7. Optical absorption spectra of macromonomers, tri-BCP and its molar blend (1:2 - pDBTTDPP:pPDIV): a) solution in CF at a concentration of 0.002mL/mg.; b) Thin film of as cast films. A lower peak intensity at 748nm is expected as it implies a lower molecular weight fraction of the pBDTTTDPP block in the tri-BCP, which is similar to the absorption spectrum of the molar blend; Photoluminescence emission spectra of the respective thin films after excitation at 633nm: c) as Cast; d) after annealing at 150°C for 15min. On a side note, no significant emission from the donor block was observed probably due to a lower absorption intensity at excitation wavelength of 633nm. (See experimental procedures for thin film preparation method).

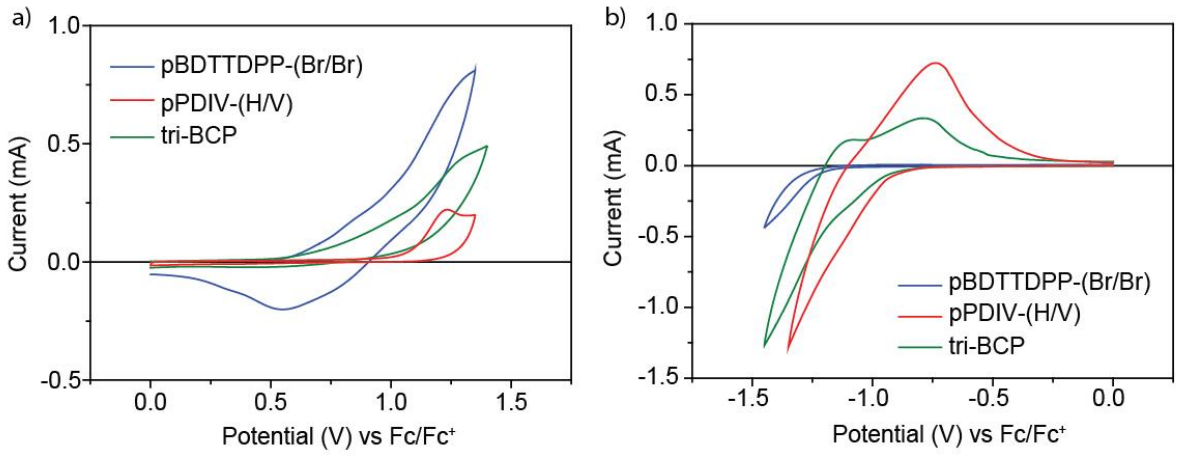

Figure S8. a) Oxidation and b) reduction of pBDTTDPP-(Br/Br), tri-BCP and pPDIV-(H/V) as determined by cyclic voltammetry.

Table S4. Summary of estimated Energy levels of pBDTTDPP-(Br/Br), pPDIV-(H/V) and tri-BCP.

OSC	[a]E_{ox}^{onset} vs Ag/AgCl	HOMO Level (eV)	[a]E_{red}^{onset} vs Ag/AgCl	LUMO Level (eV)	[b]E_g (eV)
pBDTTDPP	-0.564	-5.36[c]	-1.22	3.58[c]	1.79
pPDIV	-0.971	-5.77 [c]	-0.91	3.87 [c]	1.88
tri-BCP	-0.595	-5.39[c]	-0.92	3.89[c]	1.52

[a] See General Experimental Procedures on Cyclic voltammetry calculation of the estimated HOMO, LUMO levels and E_g. Briefly, The potential of Ag/Ag^+ reference electrode was internally calibrated by using Ferrocene/Ferrocenium (Fc/Fc^+) redox couple. The electrochemical energy levels were estimated by using the empirical formula: E_{HOMO}= −(4.80 + $E_{onset,\ ox}$) and E_{LUMO}= −(4.80 + $E_{onset,\ red}$) using the onset of the respective oxidative and reduction

[b] E_{HOMO} - E_{LUMO} = E_g.

[c]The estimated HOMO and LUMO levels of pBDTTDPP-(Br/Br), pPDIV-(H/V) corresponds closely to literature reported values (See Ref in main text)

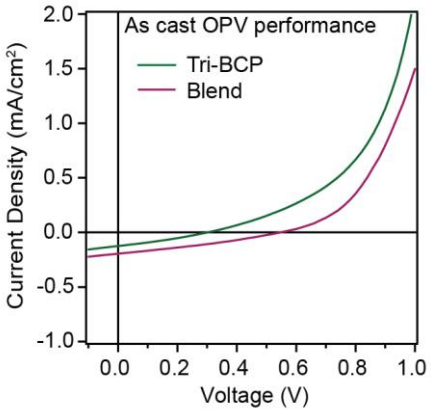

Figure S9. a) *J-V* curve of the as-cast devices of tri-BCP and the blend at a molar ratio of 1:2 – pBDTT-DPP: pPDIV

Table S5. Overall summary of photovoltaic parameter of tri-BCP and its blend at 1:2 molar ratio

BHJ	Annealing Conditions (°C)	J_{sc} (mA/cm^{-2})	V_{oc} (V)	Fill Factor (%)	PCE (%)
tri-BCP	As cast	0.13	0.34	35	0.01
	150°C	6.17	0.72	40	1.51
Molar Blend[a] pBDTTDPP: pPDIV - 1:2	As cast	0.20	0.58	33	0.04
	150°C	0.16	0.36	36	0.02

[a] Molar blend ratio is calculated based on the estimated ratio of the pBDTT-DPP and pPDIV blocks present in the tri-BCP estimated using GPC analysis.

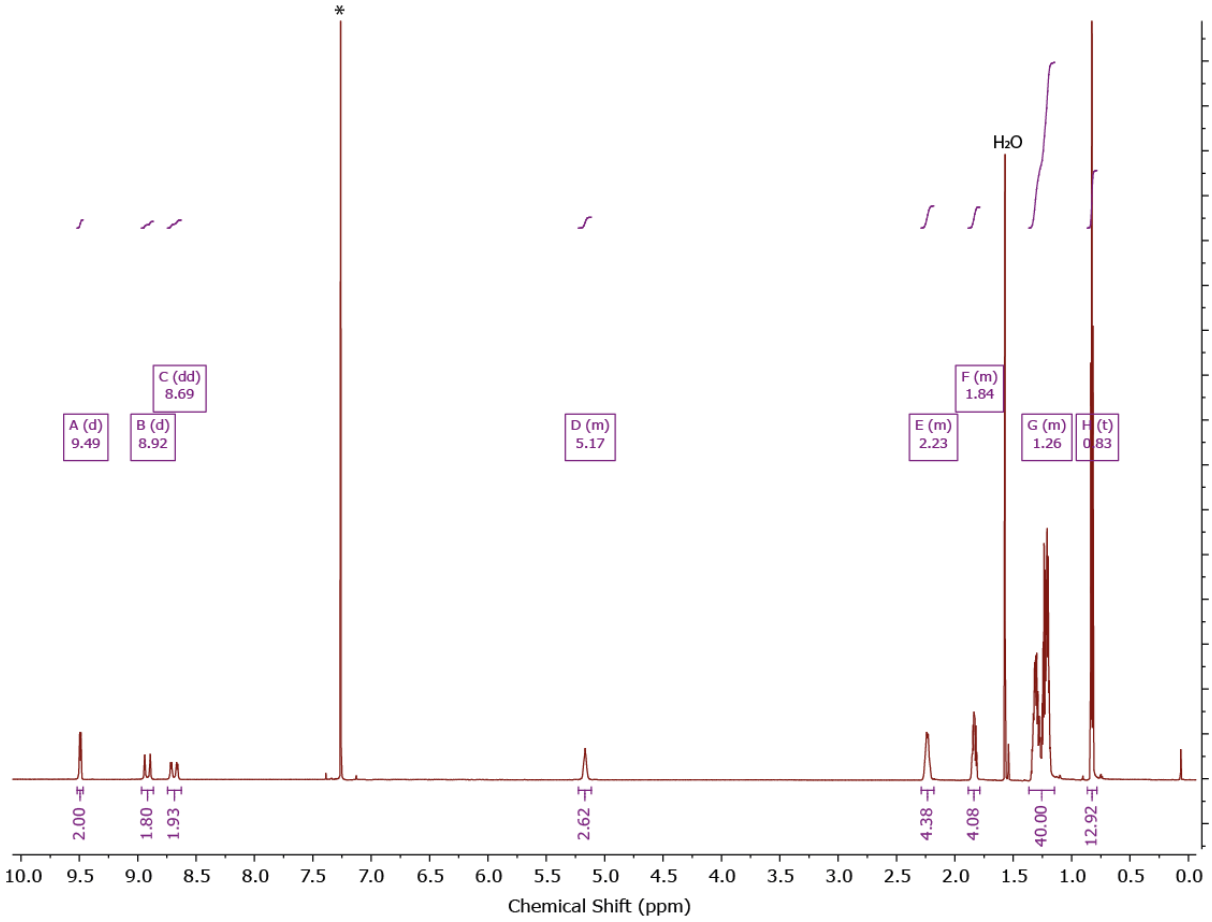

Figure S10. 800 Mhz ^{1}H NMR spectrum of Recrystallized monomer M3 (* indicates deuterated chloroform peak and a H2O impurity peak was observed at 1.58ppm.

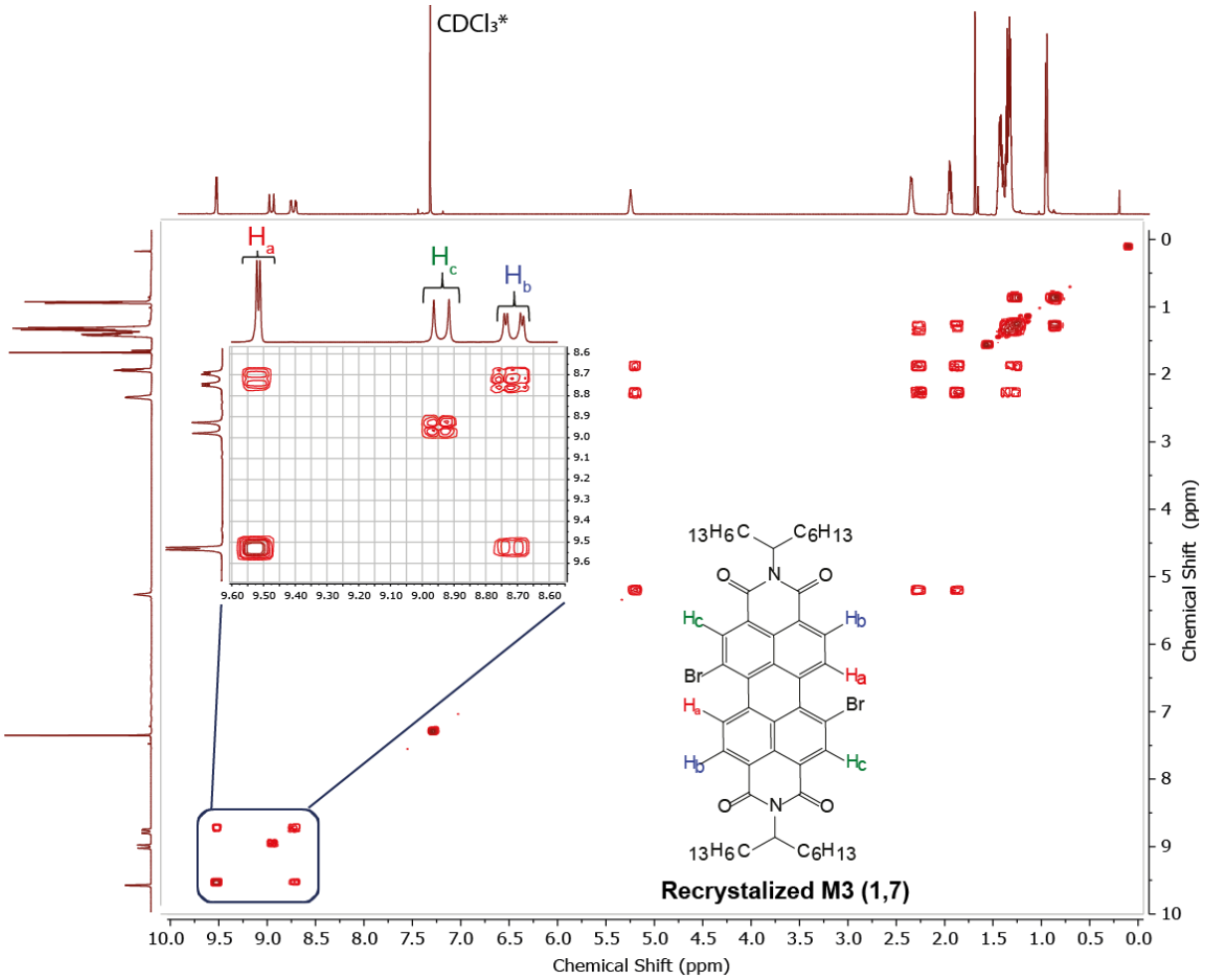

Figure S11. 800Mhz ^{1}H NMR 2D Correlation Spectroscopy (COSY) spectrum of Recrystallized monomer M3. Inset shows the magnified spectrum to indicate the assignments of the aromatic peaks on the 1,7 isomer.

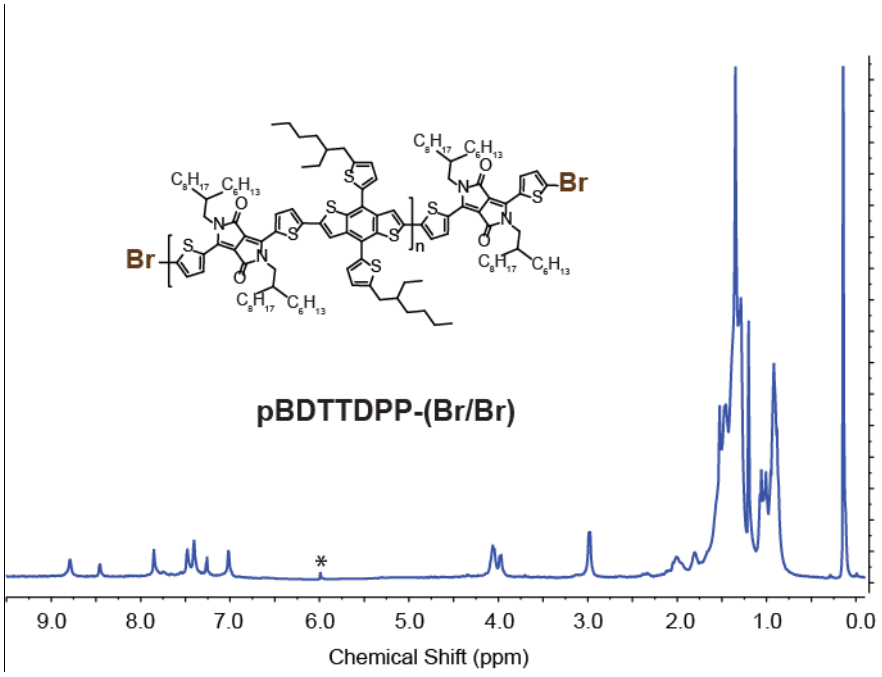

Figure S12. 800 Mhz ^{1}H NMR spectrum of pBDTTDPP-(Br/Br) (* indicates deuterated tetrachloroethane peak)

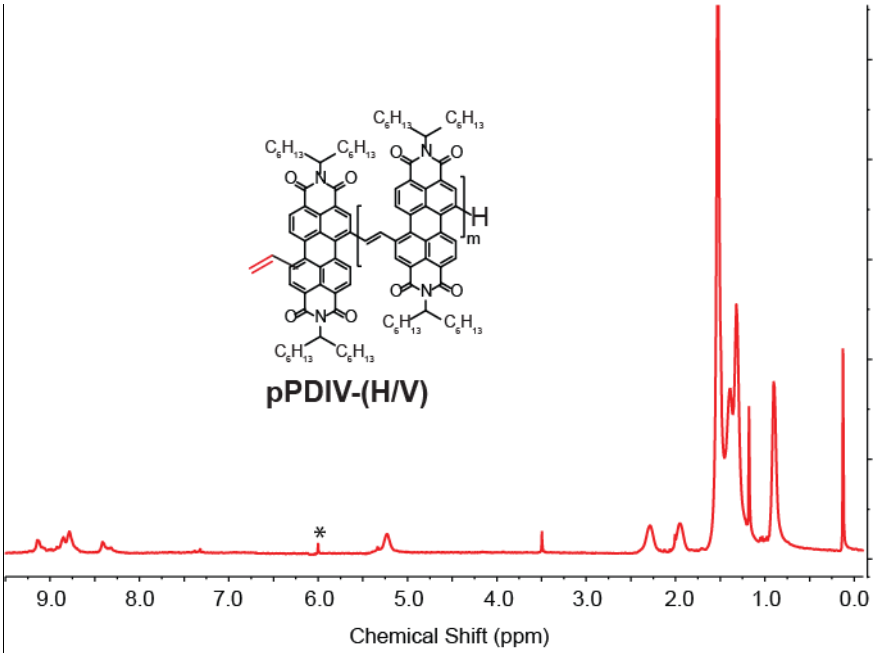

Figure S13. 800 Mhz ^{1}H NMR spectrum of pPDIV-(H/V) (* indicates deuterated tetrachloroethane peak)

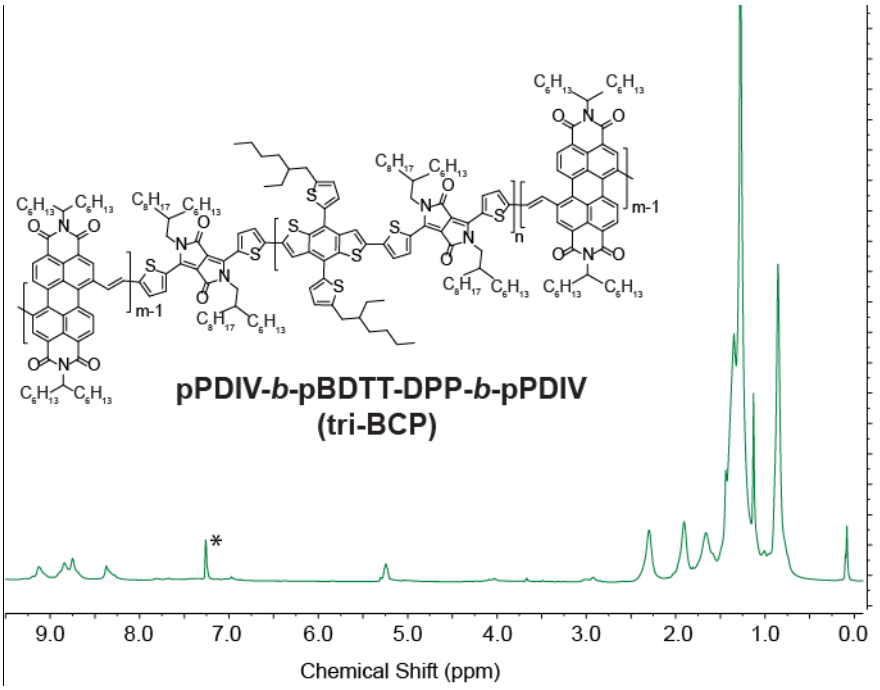

Figure S14. 800 Mhz ^{1}H NMR spectrum of tri-BCP (* indicates deuterated chloroform peak)

Supporting References.

S1. Dou, L.; Gao, J.; Richard, E.; You, J.; Chen, C.-C.; Cha, K. C.; He, Y.; Li, G.; Yang, Y., Systematic Investigation of Benzodithiophene- and Diketopyrrolopyrrole-Based Low-Bandgap Polymers Designed for Single Junction and Tandem Polymer Solar Cells. *J. Am. Chem. Soc.* **2012,** *134*, 10071-10079.

S2. Zhou, Y.; Yan, Q.; Zheng, Y.-Q.; Wang, J.-Y.; Zhao, D.; Pei, J., New Polymer Acceptors for Organic Solar Cells: The Effect Of Regio-Regularity And Device Configuration. *J. Mater. Chem. A* **2013,** *1*, 6609-6613.